All-Electron First-Principles GW+Bethe-Salpeter Program: Development & Applications

Yoshifumi NOGUCHI
Institute for Solid State Physics, The University of Tokyo
Kashiwa-no-ha, Kashiwa, Chiba 277-8581

Abstract

We have developed our original first-principles GW+Bethe-Salpeter program code employing an all-electron mixed basis approach, aiming to achieve highly accurate and reliable first-principles simulations of excited state spectra. To extend the treatable system size in this method, we redesigned and rewrote our program code as a hybrid parallel version employing both Message Passing Interface (MPI) and OpenMP. We report GW+Bethe-Salpeter calculations targeting 110-atoms systems in this report. In addition, in the first attempt world-world, we applied the *fully* first-principles GW+Bethe-Salpeter method to x-ray absorption spectra (XAS) and successfully simulated the oxygen 1s XAS for acetone and acetic acid. The calculated XAS are directly compared with the available experimental data without any artificial shifting.

1 Introduction

The first-principles Green's function method based on many-body perturbation theory beyond the framework of density functional theory (DFT) is a powerful tool in reliably simulating the excited energy spectra of a wide range of materials. One example is the GW approximation (GWA), in which GW quasiparticle energies corresponding to the poles of the one-particle Green's function directly yield the one-particle excitation energy spectra, involving the information related with the experimental (inverse) photoemission spectra. Similarly, the two-particle excitation processes can be described by an electron-hole two-particle Green's function, and the energy spectra are directly obtained from the poles of the two-particle Green's function. A standard method of determining the poles of the electron-hole two-particle Green's function from first-principles is known as the GW+Bethe-Salpeter method, in which the Bethe-Salpeter equation (BSE) is solved within the GWA. Both the GW and GW+Bethe-Salpeter methods enable us to accurately simulate excited energy spectra.

Despite great successes, these methods still have a much higher computational cost than the conventional DFT-method, scales as $O(n^3)$. The treatable system size of GW+Bethe-Salpeter is quite small. Hence, the development of a program code (or algorithm) capable in extending the treatable system size is strongly desired. For this purpose, we redesign and rewrite our program as a hybrid parallel version employing both OpenMP and Message Passing Interface (MPI) and tackle this problem.

Another topic in this report is a first-principles description of the core-electron excitations. Although information obtained from x-ray absorption spectra (XAS) is useful in understanding the properties of real materials, it is still challenging to simulate realistic XAS from first-principles without any empirical parameters, reference values from experiments,

or prior practice calculations to increase accuracy, even when the modern first-principles techniques are used rather than old-fashioned techniques based on the total-energy-difference method. The reason is that the simulation of XAS involves two difficult issues: (1) the use of an all-electron basis set capable of describing all of the electronic states from the core electron states with cusp conditions to the free electron states above vacuum level, and (2) the description on the strong electron-hole interaction, including many-body effect (so-called excitonic effect). Therefore, in contrast to the case of UV-vis absorption spectra, in which a valence electron is excited to the empty state, there are a few *fully* first-principles calculations for XAS to date. Our method, which combines an all-electron mixed basis approach and the first-principles GW+Bethe-Salpeter method, can overcome these two problems simultaneously and potentially simulates realistic XAS, which can be directly compared with those obtained experimentally.

In this report, we first introduce our method and the benchmark tests of our program, focusing on accuracy and performance, and then review recent applications.

2 Methodology

2.1 DFT

In the present method, the DFT calculation can be regarded as the starting point for subsequent calculations and adds a negligible computational cost to the entire GW+Bethe-Salpeter calculation. Therefore, we always place a priority on the developing the GW and Bethe-Salpeter components rather than the DFT component. Consequently, DFT component of our program has very limited features compared to other first-principles program packages, which are freely available online. The exchange-correlation function available in our program is only the local density approximation (LDA), and some algorithms related with the LDA that accelerate or stabilize the convergence in the self-consistent-field (SCF) loop are available. For example, band-by-band steepest decent, conjugate gradient, or block Davidson methods are available as iterative method for diagonalizing LDA Hamiltonian. To perform the iterative procedures more efficiently, we implemented recursive blocking Gram-Schmidt method of orthonormalizing wave functions and MRRR method of subspace diagonalization which is the most computationally expensive in these iterative procedures and scales as $O(n^{\,3})$. Further, as an electron-charge-mixing method, we implemented the simple or optimal linear charge mixing method and the Kerker+RMM-DIIS charge-mixing method. To stabilize the convergence for some systems with narrow band gaps, we also implemented Gaussian smearing. These algorithms allow us to perform stabilized, efficient DFT-calculations for various types of systems. The accuracy and performance of the LDA are examined in Sec. 3.

2.2 GW approximation

The GW quasiparticle energies (E_ν^{GW}) are simply given by replacing the LDA exchange-correlation potential ($\mu_{\rm xc}^{\rm LDA}$) with the GW self-energy operator (Σ^{GW}), as follow:

$$E_\nu^{GW} = E_\nu^{\rm LDA} + Z_\nu < \nu|\Sigma^{GW} - \mu_{\rm xc}^{\rm LDA}|\nu >, \quad (1)$$

$$\Sigma^{GW} = iG_0W_0 = iG_0v + iG_0(W_0 - v), \quad (2)$$

where G_0 is a one-particle Green's function, v is a bare Coulomb interaction, and W_0 is a dynamically screened Coulomb within a random phase approximation (RPA). The first term on the right hand side of Eq. (2) is the Fock-exchange term ($\Sigma^{\rm ex}$) and the second term is the GW correlation term ($\Sigma^{\rm c}$). The variables here, Σ^{GW}, W_0, and G_0, are all functions of ω; therefore, ω-integral is necessary in evaluating Eq. (2). We analytically perform this ω-integral using the Hybertsen-Louie-type generalized plasmon-pole (HL-GPP) model for the inverse of the dielectric function.

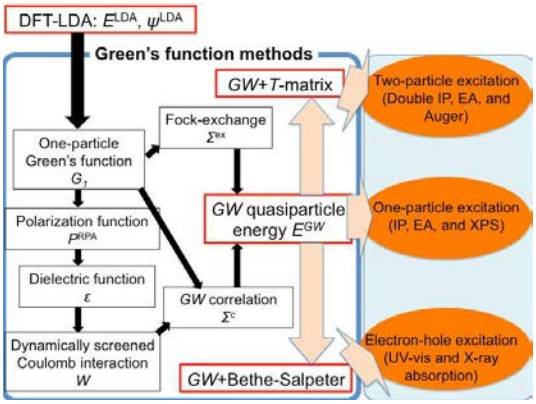

Figure 1: Flowchart of GW+Bethe-Salpeter and GW+T-matrix calculations.

2.3 Bethe-Salpeter equation

The description on the excitonic effect is significant in simulating photoabsorption spectra. To explicitly consider the excitonic effect in the present calculation, we construct the BSE and solve an ω-independent eigenvalue problem,

$$H^{\mathrm{BSE}}_{o,o';e,e'} A^i_{o,e} = \Omega_i A^i_{o,e}, \tag{3}$$

$$H^{\mathrm{BSE}}_{o,o';e,e'} \equiv (E^{GW}_e - E^{GW}_o)\delta_{o,o'}\delta_{e,e'} + \Xi^{GW}_{o,o';e,e'}, \tag{4}$$

where $\Xi^{GW}_{o,o';e,e'}$ is a matrix element of an electron-hole interaction kernel within the GWA,

$$\Xi^{GW} = \frac{\partial}{\partial G_0}(\Sigma^H + \Sigma^{GW}). \tag{5}$$

The resulting eigenvalues (Ω) and eigenvectors (A) in Eq. 3 give the excitation energy spectra and corresponding transition probabilities. We again use the HL-GPP model and analytically perform ω-integral in the BSE to take into account the dynamical excitonic effect. The details of our method are given in Ref. [1]

2.4 All-electron mixed basis program

Our program has unique features; not only does the basis set use both plane waves (PWs) and numerical atomic orbitals (AOs) but also some Green's function methods beyond the framework of DFT for simulating the excited energy spectra of the real materials are available (note that DFT-purpose calculations are outside of our scope in developing our program code because we can find a number of DFT programs online). Figure 1 shows a flowchart of the Green's function methods. Depending on the excited energy spectra of interest, our program provides three main options; the GW (or second-order Møller-Plesset perturbation, called MP2) calculation for single-particle excited energy spectra such as first-ionization potential (IP), electron affinity (EA), and band gap, the GW+Bethe-Salpeter calculation for photoabsorption spectra, and the GW+T-matrix calculation for two-particle excited energy spectra such as double IP and double EA, and Auger spectra (note that MP2 and the GW+T-matrix are outside of the scope of this review).

3 Accuracy & Performance

3.1 Benchmark test I: LDA

First, we compare our LDA results (using all-electron mixed basis) with those of the QUANTUM ESPRESSO suite [2] with three different pseudopotentials (norm conserving, ultrasoft, and PAW) to check the accuracy and convergence. Figure 2 shows (a) the LDA Kohn-Sham orbital energies at the highest occupied molecular orbital (HOMO) and the lowest unoccupied molecular orbital (LUMO), and (b) the HOMO-LUMO gap of Benzene molecule (note that because both programs, the mixed basis and ESPRESSO, can determine the vacuum level using the Coulomb cutoff technique, we can directly compare the absolute values of these orbital energies). In figure 2 (a), the Kohn-Sham orbital energies converge at same values, and we cannot see a difference among these four calculations in this energy range (horizontal axis). In figure 2 (b), a remarkable difference is found rather among the results of ESPRESSO, where the norm conserving peu-

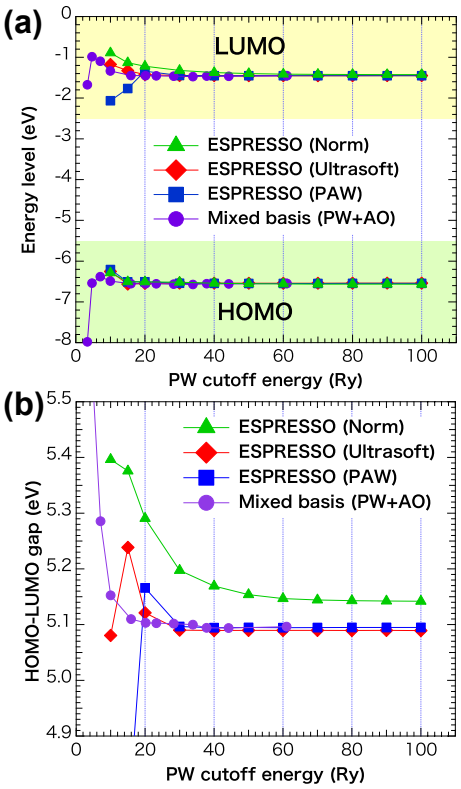

Figure 2: (a) LDA Kohn-Sham orbital energies at HOMO and LUMO levels in absolute values and (b) HOMO-LUMO gaps calculated for Benzene molecule by the present program (purple circle) and ESPRESSO with three different pseudopotentials (green triangle: norm conserving, red diamond: ultrasoft, and blue square: PAW).

dopotential conserves quite slowly against the PW cutoff energy and reaches points that differ slightly (by about 0.05 eV) from those of the other methods. In contrast, the mixed basis converges at almost same value as the ultrasoft and PAW pseudopotentials, and the required PW cutoff energy is about 15 Ry, which is almost half that given by ESPRESSO with the ultrasoft and PAW pseudopotentials (=30 Ry). These comparisons confirm the efficiency and accuracy of mixed basis method.

Table 1: Computational cost required for simulating the photoabsorption spectra of warped nanographene ($C_{80}H_{30}$) on Fujitsu FX10. Here "CPU time" is defined as "# of CPUs" × "Elapse time".

	LDA	GWA	BSE
# of CPUs	6	24	24
Elapse time (hour)	2.0	11.8	66.2
CPU time (hour)	11.9	283.2	1588.8

Table 2: Theoretical and experimental optical gaps (eV) of warped nanographene. For experimentally assigned peaks are listed here [3]. The values in "error" is discrepancies between "BSE" and "Expt.".

label	BSE	error	Expt.
S_1	2.70	0.17	2.53
S_4	2.94	0.20	2.74
S_7	3.15	0.18	2.97
S_{30}	4.00	0.16	3.84

3.2 Benchmark test II: *GW*+Bethe-Salpeter

Next, we check the *GW*+Bethe-Salpeter calculation in terms of its performance and agreement with the experiments; we choose a grossly warped nanographene ($C_{80}H_{30}$) as a benchmark test system. The computational costs required for LDA, GWA, and BSE calculations for $C_{80}H_{30}$ are listed in table 1. Although the GWA and BSE calculations require much longer CPU time than the LDA (see table 1), our hybrid parallel program with OpenMP and MPI can complete the *GW*+Bethe-Salepter calculation for $C_{80}H_{30}$ with 24 CPUs on a Fujitsu FX10 supercomputer.

As our inviolability policy for developing program code, we do not employ any algorithms that might potentially reduce the accuracy and reliability in the slightest degree, even if they can dramatically accelerate the calculation speed or reduce the computational

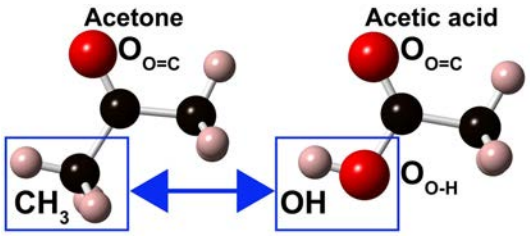

Figure 3: Atomic geometries of acetone and acetic acid optimized by B3LYP/cc-pVTZ.

Table 3: Excitation energies from oxygen 1s to LUMO (eV). Experimental values are from Refs. [11, 12].

Acetone	BSE	TD-LDA	Expt.
$O_{O=C}$	533.76	504.76	531.4
Acetic acid	BSE	TD-LDA	Expt.
$O_{O=C}$	534.74	505.34	532.13
O_{O-H}	540.34	506.64	535.44

cost. Hence, the errors found in our calculations are originated from purely theoretical considerations (note that this is an important point when we consider the development of a more accurate method beyond the present theory). We compare the BSE and experimental optical gaps for the four experimentally assigned peaks at 2.53 eV, 2.74 eV, 2.97 eV, and 3.84 eV [3]. The corresponding BSE gaps are S_1 (=2.70 eV), S_4 (=2.94 eV), S_7 (= 3.15 eV), and S_{30} (= 4.00 eV), respectively, and the remaining errors compared with the experimental values are less than 0.2 eV. Our method can handle a 110-atoms system without loss of accuracy.

4 Applications

We have applied our method to a simulation of two-particle excitation [4], simulations of UV-vis absorption spectra for systems such as sodium clusters [5], CdSe clusters [6], $M^+@C_{60}$ (where M = H, Li, Na, and K) [7], firefly luciferin [8], and defective nanographenes [9], and oxygen 1s XAS simulations [10]. We review the most recent two examples [9, 10] in following sections.

4.1 Oxygen 1s XAS of acetone and acetic acid

In this study, we applied our method to acetone and acetic acid and simulated the oxygen 1s XAS. As shown in Fig. 3, acetone has one oxygen atom chemically bonded with a carbon atom (O=C), and acetic acid has two oxygen atoms chemically bonded with a carbon atom (O=C), one of which is also bonded with a hydrogen atom (O−H). Acetone and acetic acid have the same number of electrons, and only the region in the blue rectangle in Fig. 3 is different. We see how accurately our method can simulate the absolute values of the excitation energies from oxygen 1s compared with the experimental values and whether our method can distinguish the effect of chemical bonding environment, i.e., O=C and O−H.

The calculated excitation energies corresponding to the excitation from oxygen 1s to the LUMO are listed in table 3 together with the results of time-dependent LDA (TD-LDA) calculations and the available experimental values [11, 12] for comparison. Here TD-LDA values are calculated using the Gaussian09 package [13] and the aug-cc-pVTZ basis set. Although it is well-known that the TD-LDA can determine reasonable excitation energies around UV-vis photon energy range of less than about 10 eV especially for small molecules such as acetone and acetic acid, it is obviously inaccurate for for the core electron excitations. The discrepancies between the TD-LDA and experimental values are about 26.6 eV for acetone ($O_{O=C}$), 26.8 eV for acetic acid ($O_{O=C}$), and 28.8 eV for acetic acid (O_{O-H}). This means that the static and local excitonic effect considered in TD-LDA is insufficient to describe the strong interaction between oxygen 1s core hole and excited electron. In addition,

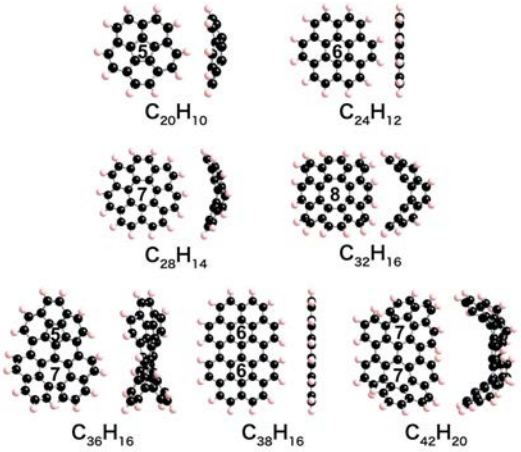

Figure 4: Atomic geometries of single and double defect molecules optimized by B3LYP/cc-pVTZ.

because the Gaussian-type-orbital (GTO) fails to describe the cusp condition of oxygen $1s$, the effect might not be negligibly small. On the other hand, the BSE, which considers a more realistic, i.e., dynamical and non-local, excitonic effect yields dramatically improved excitation energies. The remaining errors compared with the experiment are only 2.4-5.0 eV for all the cases.

Although the present results are not perfect agreement and removing these errors is not easy task, this is the first attempt worldwide to apply a *fully* first-principles GW+Bethe-Salepter method to XAS simulation. To determine the origin of the errors, we need more experience with applying this method to other systems.

4.2 Optical properties of defective nanographenes

Since Kawasumi *et al.*, successfully synthesized a grossly warped nanographene ($C_{80}H_{30}$) in 2013, it has become more important to understand the role of defects in determining the structural and electronic properties, not only because of scientific interest but also because of potential industrial applications in the future.

In this study, we applied the GW+Bethe-Salpeter method to defective and defectless nanographenes and systematically investigated the defect dependence of their properties, focusing on the optical properties such as the HOMO-LUMO gaps, optical gaps, and UV-vis absorption spectra. In particular, to see the effect of various types of the defects, such as pentagonal, heptagonal, and octagonal defect, and the effect of interaction between defects, we simulated the optical properties of the single- and double-defect molecules and the defectless counterparts, as shown in Fig. 4.

Table 4 shows the simulated optical gaps. The minimal gaps (S_1) of the single-defect molecules are all forbidden transition (dark exciton) owing to the symmetries of the corresponding wave functions, and the first dipole allowed transition (bright exciton) occurs at higher transitions, (S_n, $n \geq 2$). Although the atomic geometries of single-defect molecules: $C_{20}H_{10}$, $C_{28}H_{14}$, and $C_{32}H_{16}$, are slightly distorted from that of defectless molecule, $C_{24}H_{12}$, the high-symmetries are still retained (see Fig. 4). Actually, π-like wave functions are observed for both these single defect molecules and the defectless molecule.

As the defect changes from pentagonal to octagonal, the molecular size increases and the minimal gaps (S_1) become smaller. This tendency can be regarded as the molecular size dependence rather than a defect dependence. We cannot discuss the defect dependence for these molecules, because a strong molecular size dependence appears and hide the effect of defects.

We next discuss the interaction between defects for the double-defect molecules. Because the presence of two defects significantly distorts the atomic geometries (see Fig. 4) and also the symmetries of the corresponding wave functions, the situation differs from that of the single-defect molecules. That is, the minimal gaps, S_1, are the first dipole-allowed transition for $C_{36}H_{16}$ with pentagonal and heptagonal de-

Table 4: First dipole forbidden (dark) and allowed (bright) excitons calculated for single- and double defect-molecules and defectless molecules.

		Exciton type bright or dark	BSE gap (eV)
$C_{20}H_{10}$:	S_1	dark	3.43
	S_{12}	bright	4.46
$C_{24}H_{12}$:	S_1	dark	2.52
	S_2	bright	2.92
$C_{28}H_{14}$:	S_1	dark	2.63
	S_{27}	bright	4.40
$C_{32}H_{16}$:	S_1	dark	2.03
	S_3	bright	3.10
$C_{36}H_{16}$:	S_1	bright	2.28
$C_{38}H_{16}$:	S_1	dark	1.92
	S_2	bright	2.42
$C_{42}H_{20}$:	S_1	bright	2.24

fects, and $C_{42}H_{20}$ with two heptagons; for the defectless counter molecule, $C_{38}H_{16}$, S_1 is forbidden transition, and S_2 is the first dipole-allowed transition. The bright excitons of the defective molecules are commonly about 0.1-0.2 eV smaller values than that of the defectless molecule. This is because the excitonic effect becomes stronger for smaller atomic geometries of the defective molecules, in addition to the fact that S_1 is dipole-allowed transition.

5 Summary

We have developed a first-principles *GW*+Bethe-Salpeter program employing all-electron mixed basis approach, aiming specifically at massively parallel calculations with OpenMP and MPI and XAS simulations. Using 24 CPUs on Fujitsu FX10 supercomputer, we successfully simulated first-principles *GW*+Bethe-Salpeter calculations for 110-atoms systems without reducing accuracy and theoretical validation. Using our program, we investigated the optical properties of sodium clusters, CdSe clusters, $M^+@C_{60}$, firefly luciferin, and defective nanographenes. Furthermore, our method combining an all-electron mixed basis approach and the *GW*+Bethe-Salpeter method can simulate XAS as well as UV-vis absorption spectra within the same program code and same theoretical framework. The calculated oxygen 1*s* XAS of acetone and acetic acid show 2.4-5.0 eV errors compared with the experimental values; these errors are quite small compared with those of the TD-LDA.

References

[1] M. Rohlfing and S. G. Louie, Phys. Rev. B, **62**, 4927 (2000).

[2] P. Giannozzi *et al.*, J. Phys.: Condens. Matter **21** 395502 (2009)

[3] K. Kawasumi, Q. Zhang, Y. Segawa, L. T. Scott, and K. Itami, Nat. Chem., **5**, 739 (2013).

[4] Y. Noguchi, K. Ohno, I. V. Solovyev, and T. Sasaki, Phys. Rev. B, **81**, 165411 (2010).

[5] Y. Noguchi and K. Ohno, Phys. Rev. A, **81**, 045201 (2010).

[6] Y. Noguchi, O. Sugino, M. Nagaoka, S. Ishii, and K. Ohno, J. Chem. Phys., **137**, 024306 (2012).

[7] Y. Noguchi, O. Sugino, H. Okada, and Y. Matsuo, J. Phys. Chem. C, **117**, 15362 (2013).

[8] Y. Noguchi, M. Hiyama, H. Akiyama, and N. Koga, J. Chem. Phys., **141**, 044309 (2014).

[9] Y. Noguchi and O. Sugino, J. Chem. Phys., **142**, 064313 (2015).

[10] Y. Noguchi, M. Hiyama, H. Akiyama, Y. Harada, and N. Koga, J. Chem. Theor. Compt., **11**, 1668 (2015).

[11] T. Tamenori, O. Takahashi, K. Yamashita, T. Yamaguchi, K. Okada, K. Tabayashi, T. Gejo, and K. Honma, J. Chem. Phys., **131**, 174311 (2009).

[12] K. Tabayashi, K. Yamamoto, T. Maruyama, H. Yoshida, K. Okada, Y. Tamenori, I. H. Suzuki, T. Gejo, and K. Honma, J. Electron Spectrosc. Relat. Phenom., **184**, 134 (2011).

[13] M. J. Frisch *et al.*, *Gaussian 09* Revision **C.1**, Gaussian Inc. Wallingford CT 2010.